Effects of epitaxial strain and ordering direction on the electronic properties of GaSb/InSb and InAs/InSb superlattices

S. Picozzi and A. Continenza
Dipartimento di Fisica, Università degli Studi di L'Aquila, 67010 Coppito, L'Aquila, Italy

A. J. Freeman
Department of Physics and Astronomy and Materials Research Center, Northwestern University, Evanston, Illinois 60208-3112

(Received 28 February 1995; revised manuscript received 2 May 1995)

The structural and electronic properties in common-anion GaSb/InSb and common-cation InAs/InSb [111] ordered superlattices have been determined using the local-density total-energy full-potential linearized augmented plane-wave method. The influence of the ordering direction, strain conditions, and atomic substitution on the electronic properties of technological and experimental interest (such as energy band gaps and charge carrier localization in the different sublattices) were determined. The results show an appreciable energy band-gap narrowing compared to the band gap averaged over the constituent binaries, either in [001] ordered structures or (more markedly) in the [111] systems; moreover energy band gaps show an increasing trend as the substrate lattice parameter is decreased. Finally, the systems examined offer interesting opportunities for band-gap tuning as a function of the growth condition (about 0.7 eV in GaSb/InSb and 0.3 eV in InAs/InSb).

I. INTRODUCTION

Ternary systems based on III-V semiconductors (such as disordered alloys,[1–3] heterostructures,[4–9] or quantum well systems[10–12]) have been the subject of wide scientific interest and of accurate theoretical studies, since they could be used as fundamental components in a large class of important devices (laser diodes or infrared detectors, to name just a few).[13] In the present work, we focus our attention on superlattices (SL), whose structural, electronic, and transport properties can be opportunely tuned by varying the constituent materials, the strain, the ordering direction, or the layers thickness. To this end, we have examined the properties of interest in ultrathin [111] ordered SL, specifically in common-anion GaSb/InSb systems and in common-cation InAs/InSb systems, using the self-consistent all-electron full-potential linearized augmented plane-wave (FLAPW) method within the density functional formalism. The systems considered here are now under experimental investigation (results obtained for strained-layer InSb/GaSb quantum well,[14] $In_xGa_{1-x}Sb/GaSb$ heterostructures[15] and $InAs_{1-x}Sb_x$ alloys[16,17] have already been published); at the present time, however, we are not yet able to compare our predicted results with experimental values regarding the SL.

The appreciable mismatch between the lattice parameters of the binary constituents (5.7% in GaSb/InSb and 6.4% in InAs/InSb) gives us the opportunity to study the effects of the strain conditions on the SL electronic properties. In analogy with the common experimental approach,[14,18,19] we have considered various growth conditions for the SL, leading to different strain modes in the structure: (i) pseudomorphic growth on a substrate usually constituted by one of the binary constituents (in which the lattice constant parallel to the growth plane is taken equal to that of the bulk semiconductor composing the substrate) and (ii) a "free standing mode" (FSM), in which no constraints are imposed on the bond lengths, leading to relaxed lattice constants for the binary constituents, both different from their bulk values. The structural parameters for all of the structures considered have been chosen through total energy minimization or according to the macroscopic theory of elasticity (MTE).[20]

The choice made towards the [111] direction is encouraged by recent experimental observations[21] that suggested the spontaneous ordering along this particular axis (the so called CuPt structure), shown by some III-V alloys during vapor-phase growth. The strong influence of the ordering direction on the SL electronic properties is immediately clear if we consider the ternary SL Brillouin zones (BZ) as obtained from the binary zinc blende BZ through folding operations, which are obviously different for [111] or [001] ordered systems; the immediate consequence of this is a noticeable difference in the electronic properties.

In order to study the dependence of the electronic properties on the ordering direction, we have studied the common-anion and the common-cation systems in the three different growth conditions both in the CuAu-like (having [001] direction as growth axis) and CuPt-like structure.

Following the model proposed by Wei and Zunger,[22] we consider the SL as obtained first from an ideal virtual crystal [a common-anion (common-cation) system having the cation (anion) with intermediate properties between the two cations relative to the binary constituents].

We then introduce a perturbative potential, having a structural part (due to atomic displacements and relaxation due to epitaxial strain) and a chemical one (due to the electronegativity difference between the constituent atoms).

In order to separate the effects due to the two different terms in the expression of the potential, we have studied strained AC/AC-type systems ideally obtained by monolayer deposition of the same binary constituent (AC) along the [111] direction, in which the two different AC bond lengths are equal to those in the equivalent AC/BC SL.

We will discuss the results obtained in this work as follows: first of all, we will briefly expose the computational details and parameters used in the calculations (Sec. II); in Sec. III, our structural results will be reported for all the different systems considered. In Sec. IV, we will discuss the electronic properties of the SL, with particular attention given to the quantities of technological interest (such as energy band-gaps and crystal-field splittings) and their dependence on growth direction, atomic substitution, and strain conditions. We will also discuss the charge density distribution and, in particular, the localization of the charge carriers in the different constituents sublattices. Section V summarizes our main results and draws some conclusions.

II. METHOD OF CALCULATION

We have determined the properties of the structures considered using the density functional formalism, within the local-density approximation (LDA) (Ref. 23) exchange and correlation potential as parametrized by Hedin-Lundqvist.[24] The calculations were performed using the *ab initio* all-electron FLAPW.[25] Core electrons as well as valence ones are treated using a self-consistent procedure; the shallow Ga $3d$ and In $4d$ states are considered as valence states, for which scalar-relativistic effects are included in the self-consistent calculation, whereas spin-orbit effects are treated in a perturbative approach. For [111] ordered systems, angular momenta up to $l_{\max} = 6$ in the muffin-tin spheres (with radius $R_\alpha = 2.4$ a.u. for all the constituents atoms) and plane waves with wave vector up to $k_{\max} = 3.3$ a.u. are used, leading to about 600 basis functions.

To perform integrations in reciprocal space, a set of four special $\mathbf{k}$ points is chosen in the trigonal BZ, following the Monkhorst-Pack scheme.[26] Similar values for these computational parameters have been used for [001] ordered systems, with the only exceptions represented by $l_{\max} = 8$ and a set of three special $\mathbf{k}$ points used for the integration over the tetragonal Brillouin zone. Finally, the Broyden[27] method is used to accelerate the convergence in the self-consistent iterations.

III. STRUCTURAL PROPERTIES

The atomic ordering along the [111] direction of a SL grown on a (111) substrate results in a trigonal Bravais lattice with C_{3v}^5 (Schöenflies notation) space group.[28] The unit cell in real space contains four atoms and the origin is taken on a cation site.[29]

The free structural parameters are determined following the macroscopic theory of elasticity (MTE),[20] taking into account the elastic properties of the constituent materials, and then compared with those obtained through total-energy minimization. We observe that in each cell, there are two atoms belonging to the same chemical species (the two Sb anions in the GaSb/InSb systems and the two In cations in the InAs/InSb systems), which are not equivalent from the coordination point of view. As an example, we consider the particular case of GaSb/InSb SL, having the first $\mathrm{Sb_{Ga}}$ bound with three Ga and one In, and the second $\mathrm{Sb_{In}}$ showing a complementary situation. The total energy minimization procedure that considers all the free parameters in the unit cell as different degrees of freedom is a very onerous computational problem; this encouraged some simplifications, such as considering equal bond lengths between equal atomic species (i.e., in the common-anion system, we have chosen $d_{\mathrm{InSb_{Ga}}} = d_{\mathrm{InSb_{In}}}$), thus reducing to three the number of degrees of freedom (in-plane lattice parameter and two different bond lengths). Although this simplification is frequently used in total-energy minimizations,[29] one should be aware that this approximation results in considering an average over the two different local environments and, therefore, that the real elastic structures may differ slightly from our optimized SL's.

According to MTE, using the same notation as in Ref. 20, the structural parameters for the epilayer are determined as follows:

$$
\begin{aligned}
a_{\parallel}^{\mathrm{epi}} &= a^{\mathrm{subs}} \,, \\
a_{\perp}^{\mathrm{epi}} &= a^{\mathrm{epi}} \left[1 - D^{[111]} \left(\frac{a_{\parallel}}{a^{\mathrm{epi}}} - 1\right)\right] \,, \\
D^{[111]} &= 2 \left(\frac{c_{11} + 2\,c_{12} - 2\,c_{44}}{c_{11} + 2\,c_{12} + 4\,c_{44}}\right) \,, \\
\epsilon_{\parallel}^{\mathrm{epi}} &= \frac{a_{\parallel}}{a^{\mathrm{epi}}} - 1 \,, \\
\epsilon_{\perp}^{\mathrm{epi}} &= \frac{a_{\perp}^{\mathrm{epi}}}{a^{\mathrm{epi}}} - 1 \,,
\end{aligned}
\tag{1}
$$

where c_{ij} are the elastic constants for the bulk epilayer (we have used the experimental values reported in Ref. 30).

Through total-energy minimization of the "ideal" AC/BC unrelaxed structures [in which all the atoms are arranged in a zinc blende structure with lattice constant a—our free parameter—and with bond lengths $d_{\mathrm{AC}} = d_{\mathrm{BC}} = a\,(\sqrt{3}/4)$], we have found an in-plane lattice constant very close to the average of the bulk constituents, according to Vegard's rule. We have, thus, examined a free standing mode structure (indicated in the following as elastically relaxed or simply ER) that has this value for the in-plane lattice constant. In Table I and Table II, we report the calculated structural parameters for the ternary common-anion and common-cation systems: the $S1$ ($S2$) system is a common-anion SL grown on a GaSb (InSb) substrate, while the $S3$ ($S4$) system is a common-cation SL grown on an InAs (InSb) substrate.

TABLE I. Bond lengths (d_{GaSb} and d_{InSb} in a.u.) and strain parameters (ϵ^{GaSb} and ϵ^{InSb}) parallel and perpendicular to the growth plane for GaSb/InSb [111] and [001] ordered systems. The quantities denoted by Δ indicate percentage deviations from calculated bulk bond lengths (d_{GaSb} = 5.00 a.u. and d_{InSb} = 5.29 a.u.).

	[111]			[001]		
	El. Rel.	GaSb-subs.	InSb-subs.	El. Rel.	GaSb-subs.	InSb-subs.
d_{GaSb}	5.07	5.00	5.15	5.05	5.00	5.11
Δ_{GaSb}	+1.4%		+3.0%	+1.0%		2.2%
$\epsilon_{\parallel}^{GaSb}$	+0.029	0	+0.058	+0.029	0	+0.058
$\epsilon_{\perp}^{GaSb}$	-0.014	0	-0.028	-0.027	0	-0.053
d_{InSb}	5.22	5.16	5.29	5.25	5.24	5.29
Δ_{InSb}	-1.3%	-2.5%		-0.8%	-0.9%	
$\epsilon_{\parallel}^{InSb}$	-0.028	-0.055	0	-0.028	-0.055	0
$\epsilon_{\perp}^{InSb}$	+0.016	+0.033	0	+0.030	+0.076	0

In the case of pseudomorphic growth on a substrate, we have found general agreement between the structures obtained through total-energy minimization and those given by MTE; this fully justifies our having considered this approximation to determine the five unknown parameters in the FSM structure. Note that deviations from the results predicted by MTE occur in the case of InSb strained to GaSb or to InAs; in both these structures, total-energy minimization gives an InSb bond length that is systematically larger (within 0.6%) than the one expected according to MTE, even though the difference between the total energies for the elastic SL and for the total-energy minimal structures is very small (barely larger than the numerical uncertainty of 1 mRy/unit cell). However, this can be justified considering that, due to its elastic properties, this material could easily be out of the linear elastic region. In fact, the elastic constants for InSb are quite smaller than those for GaSb and InAs,[30] resulting in a larger effective strain—due to the mismatch—in the former case; this is also confirmed by the nonlinear behavior of the band gap as a function of the strain, as will be discussed later.

As expected from the similarity of the GaSb and InAs elastic constants[30] and bulk moduli [the experimental values are B^{InAs} = 0.579 Mb and B^{GaSb} = 0.578 Mb (Ref. 31)], we obtain similar deformations for these two constituents, respectively, in the common-anion and common-cation SL's. We also notice that strains (either parallel or perpendicular) and percentage deviations from bulk bond lengths are more pronounced in the common-cation systems, compared to the common-anion systems: this is obviously a consequence of the greater mismatch between the constituent lattice parameters in the InAs/InSb structures.

In the case of [001] ordered systems (whose structural parameters are reported in Table I and Table II, respectively, for common-anion and common-cation SL), we obtain a tetragonal Bravais lattice with D_{2d}^5 space group[28] and a unit cell in real space with four atoms (two of which are equivalent); the origin is taken on a cation (anion) site for the common-anion (common-cation) system.

The MTE relations reported in Eq. (1) are still valid for [001] ordered SL, if the parameter D is redefined as

$$D^{[001]} = 2\left(\frac{c_{12}}{c_{11}}\right). \tag{2}$$

A comparison between the [111] and [001] ordered structures (having the same chemical composition) shows that in the same growth conditions (FSM or growth on a substrate) the structural parameters are not equal. In particular, we notice larger perpendicular strains in the [001] compared to the [111] ordered structures, while the parallel strains are obviously equal in considering the

TABLE II. Bond lengths (d_{InAs} and d_{InSb} in a.u.) and strain parameters (ϵ^{InAs} and ϵ^{InSb}) parallel and perpendicular to the growth plane for InAs/InSb [111] and [001] ordered systems. The quantities denoted by Δ indicate percentage deviations from calculated bulk bond lengths (d_{InAs} = 4.96 a.u. and d_{InSb} = 5.29 a.u.).

	[111]			[001]		
	El. Rel.	InAs-subs.	InSb-subs.	El. Rel.	InAs-subs.	InSb-subs.
d_{InAs}	5.04	4.96	5.12	5.01	4.96	5.07
Δ_{InAs}	+1.6 %		+3.2%	+1.0%		2.2%
$\epsilon_{\parallel}^{InAs}$	+0.033	0	+0.066	+0.033	0	+0.066
$\epsilon_{\perp}^{InAs}$	-0.019	0	-0.038	-0.036	0	-0.072
d_{InSb}	5.21	5.14	5.29	5.24	5.22	5.29
Δ_{InSb}	-1.5%	-2.8%		-0.9%	-1.3%	
$\epsilon_{\parallel}^{InSb}$	-0.031	-0.062	0	-0.031	-0.062	0
$\epsilon_{\perp}^{InSb}$	+0.019	+0.037	0	+0.033	+0.078	0

TABLE III. Calculated electronic energy levels (in eV) with respect to the VBM for the [111] SL (neglecting s.o. coupling). The superscripts (1) and (2) indicate the two states involved in the repulsion mechanism. The state multiplicity is given in parentheses.

SL state	ZB state	GaSb/InSb			InAs/InSb		
		ER	$S1$	$S2$	ER	$S3$	$S4$
$\Gamma_{1c}^{(2)}$	L_{1c}	0.50	0.70	-0.20	0.79	1.04	0.36
$\Gamma_{1c}^{(1)}$	Γ_{1c}	-0.81	-0.64	-1.47	-1.02	-0.95	-1.42
$\Gamma_{3v}^{(2)}$	Γ_{15v}	0(2)	0(2)	-0.42(2)	0(2)	0(2)	-0.18(2)
Γ_{1v}	Γ_{15v}	-0.11	-0.59	0	-0.21	-0.77	0
$\Gamma_{3v}^{(1)}$	L_{3v}	-1.31(2)	-1.35(2)	-1.68(2)	-1.38(2)	-1.46(2)	-1.50(2)

same growth conditions; what we find is thus a smaller deviation from bulk bond lengths, due to a more effective relaxation.

IV. ELECTRONIC PROPERTIES

A. Electronic levels

The determination of the SL electronic energy levels is a fundamental point for most of the properties of interest in the systems considered. In Table III, we report the calculated electronic levels (with a numerical uncertainty of $\pm$ 0.04 eV, equal for all the energies reported in the present work, unless otherwise specified) at the BZ center (Γ), for the different [111] ordered systems considered (free standing mode and pseudomorphic growth on the two substrates), both for the common-anion and for the common-cation systems. We also report the zinc blende state from which the SL state derives through folding the fcc Brillouin zone back into the smaller ternary trigonal zone.

The splitting, $\Delta_{\rm CF}$, of the triply degenerate Γ_{15v} zinc blende state is due to the non-cubic crystal field and is conventionally taken positive if the doubly degenerate state $\Gamma_{3v}^{(2)}$ has a higher energy compared to the state Γ_{1v}. As can be seen from Table III, we obtain a negative $\Delta_{\rm CF}$ in the case of GaSb (InAs) strained to InSb for common-anion (cation) systems—corresponding to an in-plane extensive strain $\epsilon_{\|}$—whereas the complementary case [pseudomorphic growth on a GaSb-substrate (InAs substrate)] and the free standing mode produce a positive $\Delta_{\rm CF}$.

The introduction of spin-orbit coupling removes the double degeneracy of the $\Gamma_{3v}^{(2)}$ state and yields the electronic energy levels illustrated in Fig. 1 as a function of the substrate lattice constant. The topmost valence bands (E_1, E_2, E_3) have been labeled according to the "quasicubic" model[32] (taking the center of gravity of the SL valence bands as zero);

$$E_1 = +\tfrac{1}{3}(\Delta_{\rm s.o.} + \Delta_{\rm CF})$$
$$E_{2,3} = -\tfrac{1}{6}(\Delta_{\rm s.o.} + \Delta_{\rm CF}) \pm \tfrac{1}{2}\{(\Delta_{\rm s.o.} + \Delta_{\rm CF})^2 - \tfrac{8}{3}\,\Delta_{\rm s.o.}\,\Delta_{\rm CF}\}^{1/2},$$

considering $\Delta_{\rm CF}$ as obtained from Table III and $\Delta_{\rm s.o.}$ for the SL as the value averaged over the equivalent calculated[33] quantities for the binary constituents. (Even neglecting the $\Delta_{\rm s.o.}$ negative bowing, occurring in the common-cation SL,[22] it is possible to uniquely identify

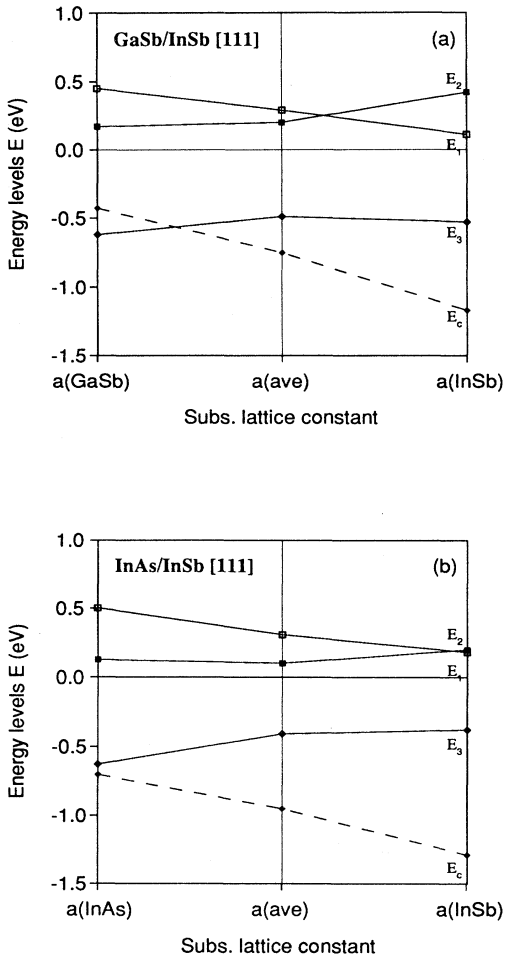

FIG. 1. Calculated highest valence band energy levels (E_1, E_2, and E_3) and lowest conduction state (E_c) at Γ versus substrate lattice constant for the [111] (a) common-anion and (b) common-cation SL's considered. The center of gravity of the topmost valence bands is taken as zero.

TABLE IV. Calculated electronic energy levels (in eV) with respect to the VBM for the [001] SL (neglecting s.o. coupling). The superscripts (1) and (2) indicate the two states involved in the repulsion mechanism. The state multiplicity is given in parentheses.

SL state	ZB state	GaSb/InSb			InAs/InSb		
		ER	$S1$	$S2$	ER	$S3$	$S4$
$\Gamma_{1c}^{(2)}$	X_{1c}	1.12	1.26	0.78	1.46	1.54	1.01
$\Gamma_{1c}^{(1)}$	Γ_{1c}	-0.49	-0.43	-0.77	-0.68	-0.69	-0.96
$\Gamma_{5v}^{(2)}$	Γ_{15v}	0(2)	0(2)	-0.20(2)	0(2)	0(2)	-0.25(2)
Γ_{4v}	Γ_{15v}	-0.07	-0.41	0	-0.06	-0.46	0
$\Gamma_{5v}^{(1)}$	X_{5v}	-2.52(2)	-2.52(2)	-2.71(2)	-2.46(2)	-2.46(2)	-2.70(2)

the SL levels with the "quasicubic" ones, which differ at most by 0.05 eV.) From Fig. 1 we notice that the E_1 and E_c (the lowest conduction state) levels show an almost linear behavior as a function of the substrate lattice constant, while the other valence band states show a more complex trend, due to the interplay between crystal-field and s.o. effects (see the cross-over between the E_1 and E_2 states).

In Table IV, we report the relevant electronic energy levels for the CuAu systems at Γ; the notation is analogous to that of Table III, where folding relations of the fcc Brillouin zone in the now tetragonal ternary zone involve the zinc blende states, as indicated in the Table. The trend in the signs of the crystal-field splittings Δ_{CF} is similar to that evidenced in the [111] ordered systems (see Table IV).

The general underestimation of the band-gap energy in LDA has stimulated many attempts to solve this problem, but correction algorithms[34–36] need an extraordinary computational effort in the SL case; thus, our LDA band-gap energy (E_{gap}^{LDA}) was corrected starting from the experimental data of the binary constituents.[37] Due to a lack of experimental band gaps regarding strained binaries, we have fitted the calculated values obtained for each binary in different strain conditions (i.e., tetragonal and trigonal), assuming a linear trend for the band-gap energy as a function of the in-plane strain $\epsilon_{\|}$: $E_{gap}^{LDA}(\epsilon_{\|}) = E_{gap}^{LDA}(0) + \alpha\,\epsilon_{\|}$, where $E_{gap}^{LDA}(0)$ is the binary equilibrium calculated band gap [a parabolic trend $E_{gap}^{LDA}(\epsilon_{\|}) = E_{gap}^{LDA}(0) + \alpha\,\epsilon_{\|} + \beta\,\epsilon_{\|}^2$ has been used for InSb, which is assumed to be out of the linear region]. Once we determined the coefficient α, we translated the curve so that it becomes $E_{gap}^{emp}(\epsilon_{\|}) = E_{gap}^{expt}(0) + \alpha\,\epsilon_{\|}$, where $E_{gap}^{expt}(0)$ is the binary equilibrium experimental band gap. We have thus used these empirical values to obtain the empirical band-gap energy averaged over the strained binaries ($\langle E_{gap}^{emp}\rangle$). Summing this quantity to the correction [$\delta = E_{gap}^{LDA}(SL) - \langle E_{gap}^{LDA}\rangle$], we have finally obtained the predicted band-gap energy in the SL ($E_{gap}^{emp}(SL)$) with a numerical uncertainty of $\pm$ 0.05 eV. Although this procedure is empirical, it is expected to give good estimates of the real band gaps, since it is well known that while the band gap is strongly underestimated, the band-gap behavior as a function of pressure is always very well reproduced by LDA.[33]

We report in Tables V and VI (respectively, for [111] and [001] ordered structures), the band-gap energies as obtained from LDA self-consistent unperturbed calculations (E_{gap}^{unp}), with the introduction of the perturbation due to spin-orbit coupling (E_{gap}^{LDA}) and with the correction starting from experimental data (E_{gap}^{emp}). From these Tables, we first notice that for all the systems considered, we find a negative E_{gap}^{LDA} [due to an inversion which causes the conduction band minimum (CBM) to lie below the valence band maximum (VBM)]. Furthermore, we observe that the larger the substrate lattice parameter, the smaller the band-gap energy (either in common-anion or in common-cation systems).

A comparison between Table V and Table VI confirms the trend predicted by Wei and Zunger[37] for the energy band gap:

$$E_{gap}^{[111]} < E_{gap}^{[001]} < E_{gap}^{ave} \qquad (3)$$

where $E_{gap}^{[111]}$ and $E_{gap}^{[001]}$ are the band-gap energies, respectively, in the [111] and in the [001] ordered struc-

TABLE V. Band-gap energies (in eV) for GaSb/InSb [111] systems and InAs/InSb [111] obtained from unperturbed LDA calculations (E_{gap}^{unp}), with the introduction of spin-orbit coupling (E_{gap}^{LDA}) and corrected starting from experimental data (E_{gap}^{emp}). We also report the calculated bowing parameter ($b_{gap}^{[111]}$) for the different systems considered.

	GaSb/InSb			InAs/InSb		
	ER	$S1$	$S2$	ER	$S3$	$S4$
E_{gap}^{unp}	-0.81	-0.64	-1.47	-1.02	-0.95	-1.42
E_{gap}^{LDA}	-1.05	-0.90	-1.59	-1.26	-1.20	-1.49
E_{gap}^{emp}	0.05	0.20	-0.47	-0.26	-0.21	-0.51
$b_{gap}^{[111]}$	1.92	1.32	4.08	2.42	2.18	3.34

TABLE VI. Band-gap energies (in eV) for GaSb/InSb [001] systems and InAs/InSb [001] obtained from unperturbed LDA calculation ($E_{\rm gap}^{\rm unp}$), with the introduction of spin-orbit coupling ($E_{\rm gap}^{\rm LDA}$) and corrected starting from experimental data ($E_{\rm gap}^{\rm emp}$). We also report the calculated bowing parameter ($b_{\rm gap}^{[001]}$) for the different systems considered.

	GaSb/InSb			InAs/InSb		
	ER	$S1$	$S2$	ER	$S3$	$S4$
$E_{\rm gap}^{\rm unp}$	-0.49	-0.43	-0.77	-0.68	-0.69	-0.96
$E_{\rm gap}^{\rm LDA}$	-0.74	-0.69	-0.96	-0.88	-0.89	-1.07
$E_{\rm gap}^{\rm emp}$	0.33	0.41	0.13	0.11	0.10	-0.09
$b_{\rm gap}^{[001]}$	0.68	0.48	1.56	0.90	0.94	1.66

tures, while $E_{\rm gap}^{\rm ave}$ is the band-gap average energy taken over the binary constituents [the calculated values of the LDA band-gap energy for the binary constituents are $E_{\rm gap}^{\rm LDA}({\rm GaSb}) = -0.47$ eV, $E_{\rm gap}^{\rm LDA}({\rm InSb}) = -0.67$ eV, and $E_{\rm gap}^{\rm LDA}({\rm InAs}) = -0.63$ eV].

As is well-known,[22] band folding in the superstructures causes a repulsion between two binary electronic states of different symmetries, folded on a state of the same symmetry in the ternary phase and coupled through the perturbative potential mentioned in Sec. I [in Tables III and IV the superscripts (1) and (2) indicate the two states involved in the repulsion mechanism]. One of its interesting effects is the band-gap narrowing, compared to the equivalent quantity averaged over the binary constituents [as confirmed by the second inequality in Eq. (3)]. The amount of this effect[22] is inversely proportional to the difference $[\epsilon(\Gamma_{1c}) - \epsilon(L_{1c})]$ (in the [111] structure) or to the difference $[\epsilon(\Gamma_{1c}) - \epsilon(X_{1c})]$ (in the [001] structure); this difference is smaller in the [111] structure, causing a more striking band-gap narrowing than in the [001] structure [as shown by the first inequality in Eq. (3)]. These observations are confirmed by the calculated values for the band-gap bowing parameters [defined, in analogy with the 50%-50% alloys, as $b_{\rm gap} = 4(E_{\rm gap}^{\rm ave} - E_{\rm gap})$] reported in Tables V and VI: we obtain a larger bowing in the [111] structures compared to the [001] ones and, looking at the constituent chemical species, we can say that the bowing in common-cation systems is larger than in the common-anion ones.

The band-gap trend as a function of the substrate lattice constant and its dependence on the ordering direction have been illustrated in Fig. 2, where we report the LDA band gap ($E^{\rm LDA}$—solid line) and corrected band gap ($E^{\rm emp}$—dashed line), as a function of the substrate lattice constant for GaSb/InSb [Fig. 2(a)] and InAs/InSb [Fig. 2(b)]. A comparison between the SL energy band gaps and the average value ($E_{\rm ave}$) of the experimental (LDA) band gap in the pure binaries—indicated by the filled (empty) circles—clearly shows the band-gap narrowing effect.

Tables V and VI also show that the crystal-field splittings in the [111] ordered structures are always bigger than in the [001] structures in the same growth conditions, with the only exception represented by the $S4$ system, which has a smaller $\Delta_{\rm CF}$ compared to the other structures. This apparently strange behavior can be explained by considering that the $\Gamma_{3v}^{(2)}$ state interacts with the lower $\Gamma_{3v}^{(1)}$ state, resulting in an upward shift (an effect relevant only in the common-cation SL's); furthermore, in the $S4$ system, the VBM is a Γ_{1v} state, which is only slightly involved in the level repulsion mechanism. Thus, the stronger the level repulsion, the larger the $\Gamma_{3v}^{(2)}$

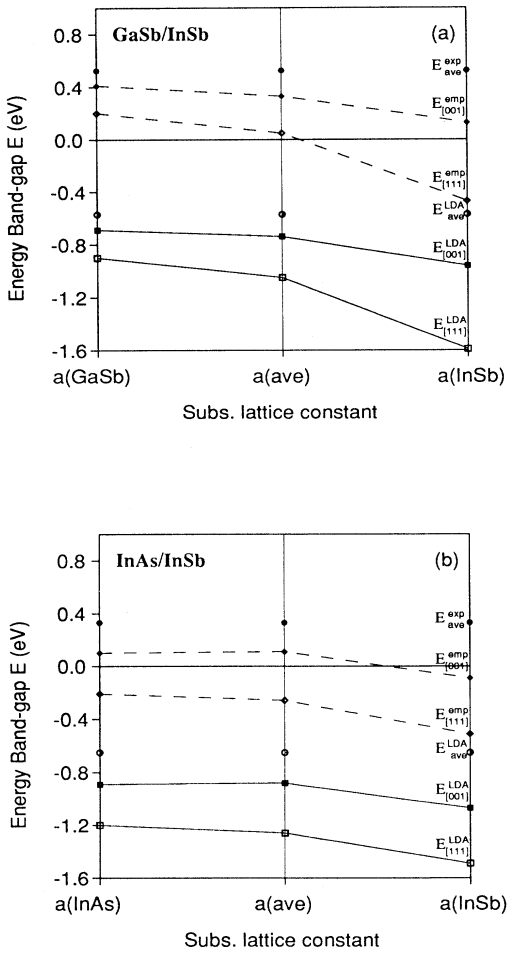

FIG. 2. LDA band gap ($E^{\rm LDA}$ — solid line) and corrected band gap ($E^{\rm emp}$ — dashed line), as a function of the substrate lattice constant for the [111] and [001] (a) GaSb/InSb SL's and (b) InAs/InSb SL's. Filled (empty) circles indicate the average value ($E_{\rm ave}$) of the experimental (LDA) band-gap in the pure binaries.

TABLE VII. Band-gap energies E_{gap}^{LDA}, spin-orbit coupling included, and crystal-field splittings Δ_{CF} (in eV) for common-anion systems.

	GaSb/InSb			GaSb/GaSb			InSb/InSb		
	ER	$S1$	$S2$	ER	$S1$	$S2$	ER	$S1$	$S2$
E_{gap}^{LDA}	-1.05	-0.90	-1.59	-1.15	-1.14	-1.66	-0.34	-0.26	-0.88
Δ_{CF}	0.11	0.59	-0.42	0.19	0.58	-0.42	0.14	0.57	-0.50

upward shift and the smaller Δ_{CF} becomes: this observation is, thus, a further proof of the validity of the band repulsion model.

We observe that in the [111] ordered SL's the band-gap energy is determined by the difference in energy between the VBM—slightly localized on the anion belonging to the InSb monolayer (as will be clearly shown in the next section)—and the CBM—strongly localized on the GaSb (InAs) sublattice in the common-anion (cation) superlattice. Thus, we could think of GaSb/GaSb-type systems as common-anion SL's in which we substitute the InSb monolayer with a GaSb monolayer. We would expect in this case a small modification of the band-gap energy, since the VBM will no longer be localized on the Sb belonging to the InSb sublattice, but rather on the Sb belonging to a GaSb sublattice; therefore, this will be only a second order effect. Our prediction is confirmed by the calculated band-gap energies (spin orbit included) reported in Table VII (second column), which prove the almost total independence of the VBM on the cationic substitution; the change of the band-gap energy in the different structures is thus caused by the structural term in the perturbative SL potential rather than by the chemical term. An equivalent interpretation considers the InSb/InSb-type systems as SL's in which we have substituted the GaSb monolayer (where the CBM is strongly localized) with an InSb monolayer. In this case, the cationic substitution implies the chemical alteration of one of the atomic species (Ga) on which the wave function is strongly localized; thus, what we expect, is an appreciable change in the band-gap energy, as confirmed by the third column in Table VII (from which we notice the E_{gap}^{LDA} increase). An analogous trend is observed for the common-cation systems, where InAs has now susbstituted the GaSb as the InSb partner in the SL (see second and third column in Table VIII).

The trend in the crystal-field splitting is strongly dependent on the class of systems considered. In fact, in the common-anion systems, this quantity is almost independent of the cationic substitution (as expected, because of the anionic character of the VBM, localized on the Sb atom). In this case, the chemical term of the potential existing in the SL has very little effect on Δ_{CF}, compared to the structural term (see Table VII). On the other hand, in common-cation systems anionic substitution has a strong effect on the crystal-field splitting and the chemical term in the SL potential is now much more important than before, even though the structural term still has a strong effect on Δ_{CF} (see Table VIII).

B. Charge density distribution

One of the main effects of the perturbative potential in the SL (in particular, of its chemical term, due to differences in the constituent atom's orbital energies[9]) is the localization of the charge density in one of the constituent monolayers, which varies from state to state. As an obvious consequence, this effect causes the confinement of the charge carriers (holes or electrons, respectively, for valence or conduction states) in a different sublattice.

In order to better clarify the character relative to the different states of interest, their angular decomposition—for the common-anion systems in the three growth conditions considered—is reported in Table IX (we do not report the equivalent table for InAs/InSb, since this system is very similar to the previous one, as far as the charge decomposition is concerned). Referring to the charge density of the Γ_{1v} state, we notice, in particular, the growing s character on the InSb monolayer and the decreasing p character on the In atom as the substrate lattice parameter is increased; at the same time, the s charge density on the GaSb sublattice decreases, while the p charge grows on the Ga atom.

We report in Fig. 3(a) distribution for the Γ_{1v} state for the GaSb/InSb ER systems, drawn the same for all the charge densities reported in this work in a plane perpendicular to the atomic layers. This state comes from p_z orbitals (as we can see from the typical "butterfly" shape along the vertical growth z direction) and shows a strong bonding character, between different monolayers and within each monolayer.

In Fig. 3(b), we report the charge density distribution relative to the $\Gamma_{3v}^{(2)}$ (VBM) state for the common-anion system in its elastically relaxed structure, where the lo-

TABLE VIII. Band-gap energies E_{gap}^{LDA}, spin-orbit coupling included, and crystal-field splittings Δ_{CF} (in eV) for common-cation systems.

	InAs/InSb			InAs/InAs			InSb/InSb		
	ER	$S3$	$S4$	ER	$S3$	$S4$	ER	$S3$	$S4$
E_{gap}^{LDA}	-1.26	-1.20	-1.49	-1.26	-1.24	-1.44	-0.29	-0.25	-1.09
Δ_{CF}	0.21	0.77	-0.18	0.14	0.57	-0.39	0.11	0.68	-0.47

TABLE IX. Angular decomposition relative to the muffin-tin charge density [for s (Q_s) and p (Q_p) components] of the different states, neglecting s.o. coupling, for the GaSb/InSb [111] systems.

State		$S1$				ER				$S2$			
		Ga	Sb	In	Sb	Ga	Sb	In	Sb	Ga	Sb	In	Sb
Γ_{1v}	Q_s	0.065	0.057	0.006	0.005	0.003	0.001	0.014	0.017	0.007	0.001	0.045	0.023
	Q_p	0.037	0.187	0.060	0.134	0.040	0.218	0.048	0.184	0.074	0.115	0.014	0.241
$\Gamma_{3v}^{(2)}$	Q_s	0.000	0.000	0.000	0.000	0.000	0.000	0.000	0.000	0.000	0.000	0.000	0.000
	Q_p	0.023	0.122	0.061	0.321	0.025	0.117	0.063	0.306	0.026	0.114	0.063	0.294
$\Gamma_{1c}^{(1)}$	Q_s	0.262	0.177	0.074	0.072	0.345	0.232	0.047	0.045	0.349	0.217	0.031	0.030
	Q_p	0.019	0.027	0.002	0.063	0.005	0.019	0.006	0.001	0.011	0.031	0.005	0.001
$\Gamma_{1c}^{(2)}$	Q_s	0.028	0.008	0.188	0.161	0.008	0.000	0.228	0.180	0.000	0.003	0.223	0.180
	Q_p	0.073	0.024	0.000	0.025	0.057	0.006	0.001	0.052	0.001	0.106	0.033	0.004

calization of the charge density in the InSb sublattice is particularly evident. We notice that this peculiarity is much more enhanced in the common-cation system (not shown), as a probable consequence of the anionic character of this state: in fact, what we expect in the common-cation system is for the Sb atom to draw more charge than the As atom. We have found that the charge density distribution in this state is not strongly influenced by the strain conditions, as can be seen from Table IX.

The calculated charge density distribution for the first conduction state $\Gamma_{1c}^{(1)}$ (CBM), relative to the common-anion elastically relaxed system, is presented in Fig. 4(a). What is relevant in this state is the strong localization of the charge density in the GaSb monolayer (a similar behavior is shown by the common-cation ER system, where the charge density is concentrated on the InAs monolayer).

The localization emphasized above becomes more pronounced as the substrate lattice parameter is increased: the charge density distribution concentrates more and more in the GaSb monolayer (InAs monolayer), while at the same time the InSb monolayer becomes charge-depleted (as confirmed by Table IX). The second conduction state, $\Gamma_{1c}^{(2)}$, shows a complementary trend, owing to the charge density distribution that is more and more concentrated on the InSb sublattice as the substrate lattice parameter is increased [as we notice from Fig. 4(b) for the common-anion elastically relaxed system; this behavior is similar to the common-cation systems].

As a consequence of these observations, in all these structures we have a direct gap in reciprocal space, while we obtain a "spatially indirect" gap, due to the localization of the $\Gamma_{3v}^{(2)}$ state (VBM) on the InSb sublattice and of the $\Gamma_{1c}^{(1)}$ state (CBM) on the GaSb (InAs) sublattice in the common-anion (common-cation) SL.

V. CONCLUSIONS

Ab initio FLAPW calculations, based on density functional theory within LDA, have been performed in order to determine the electronic properties of ultrathin SL's. In particular, we have studied a common-anion GaSb/InSb system and a common-cation InAs/InSb system, ordered along two different ([111] and [001]) directions .

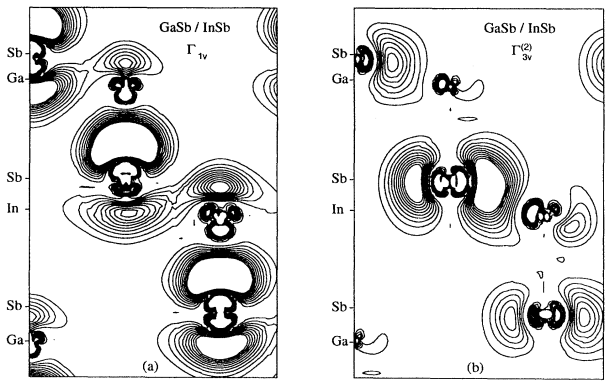

FIG. 3. Charge density distribution (in units of 0.5 e/unit cell) for the (a) Γ_{1v} state and for the (b) $\Gamma_{3v}^{(2)}$ state in the elastically relaxed [111] ordered common-anion structure.

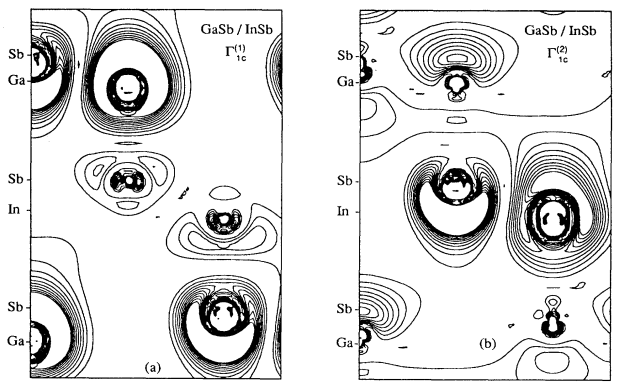

FIG. 4. Charge density distribution (in units of 0.5 e/unit cell) for the (a) $\Gamma_{1c}^{(1)}$ (CBM) state and for the (b) $\Gamma_{1c}^{(2)}$ state in the elastically relaxed [111] ordered common-anion structure.

The relevant results obtained for these structures can be summarized as follows.

(1) Both the GaSb/InSb and InAs/InSb systems show a direct gap ($E_{\rm gap}^{[111]}$), which is smaller than the average band-gap energy ($E_{\rm gap}^{\rm ave}$) taken over the binary constituents: the dependence of this quantity on the ordering direction is expressed by the relation: $E_{\rm gap}^{[111]} < E_{\rm gap}^{[001]} < E_{\rm gap}^{\rm ave}$.

(2) Both common-anion and common-cation systems show a decreasing band-gap energy as the substrate lattice parameter is increased.

(3) The structures studied offer interesting opportunities for band-gap tuning as a function of growth conditions; the range in which the gap varies is as large as 0.7 eV in GaSb/InSb type systems and 0.3 eV in InAs/InSb systems.

(4) In the common-anion (common-cation) systems, the marked charge density localization of the CBM on the GaSb (InAs) monolayer and of the VBM on the InSb monolayer causes the gap to be "spatially indirect."

(5) In the case of free standing mode elastically relaxed structures, we obtain a band-gap value of 0.05 ± 0.05 eV in the common-anion system (semiconducting properties) and of -0.26 ± 0.05 eV in the common-cation system (semimetallic properties).

ACKNOWLEDGMENTS

We thank B.W. Wessels for stimulating discussions and a careful reading of the manuscript. Work at Northwestern University supported by the MRL Program of the National Science Foundation, at the Materials Research Center of Northwestern University, under Award No. DMR-9120521, and by a grant of computer time at Pittsburgh Supercomputing Center.

[1] D.J. Arent *et al.*, Appl. Phys. Lett. **62**, 1806 (1993).
[2] S.H. Wei, B. Laks, and A. Zunger, Appl. Phys. Lett. **62**, 1937 (1993).
[3] V. Lemos, C. Vasquez-Lopez, and F. Cardeira, Superlatt. Microstruct. **13**, 1891 (1993).
[4] A. Continenza, S. Massidda, and A.J. Freeman, Phys. Rev. B **42**, 3469 (1990).
[5] N.E. Christensen and I. Gorczyka, Phys. Rev. B **50**, 4397 (1994).
[6] N.G. Anderson and S. Jones, J. Appl. Phys. **70**, 4342 (1991).
[7] N. Tit, M. Peressi, and S. Baroni, Phys. Rev. B **48**, 17 607 (1993).
[8] A. Rubio, J.L. Corkill, and M.L. Cohen, Phys. Rev. B **49**, 1952 (1994).
[9] A. Franceschetti, S.H. Wei, and A. Zunger, Phys. Rev. B **50**, 8094 (1994).
[10] S. Vlaev, R.V. Velasco, and F. García Moliner, Phys. Rev. B **50**, 4577 (1994).
[11] A.D. Prins *et al.*, Phys. Rev. B **47**, 2191 (1993).
[12] L.Q. Qian and B.W. Wessels, J. Appl. Phys. **75**, 3024 (1993).
[13] See, for example, *Materials for Infrared Detectors and Sources*, edited by R. Farrow, J.F. Schetzina, and J.T. Cheung, MRS Symposia Proceedings No. 90 (Materials Research Society, Pittsburgh, 1987).
[14] L.Q. Qian and B.W. Wessels, Appl. Phys. Lett. **63**, 628 (1993).
[15] L.Q. Qian and B.W. Wessels, J. Vac. Sci. Technol. **11**, 1652 (1993).
[16] S. Elies, A. Krier, I.R. Cleverley, and K. Singer, J. Phys. D **26**, 159 (1993).
[17] S.R. Kurtz, L.R. Dawson, R.M. Biefeld, D.M. Follstaedt, and B.L. Doyle, Phys. Rev. B **46**, 1909 (1992).
[18] C. Ohler *et al.*, Phys. Rev. B **50**, 7833 (1994).
[19] A. Bensaada *et al.*, J. Appl. Phys. **75**, 3024 (1993).
[20] C.G. Van de Walle, Phys. Rev. B **39**, 1871 (1988).
[21] For a review see A. Zunger and S. Mahajan, *Handbook of Semiconductors*, 2nd ed. (Elsevier, Amsterdam, 1994), Vol. 3.
[22] S.H. Wei and A. Zunger, Phys. Rev. B **39**, 3279 (1989).
[23] P. Hohenberg and W. Kohn, Phys. Rev. **136**, B864 (1964); W. Kohn and L.J. Sham, *ibid.* **140**, A1133 (1965).
[24] L. Hedin and B.I. Lundqvist, J. Phys. C. **4**, 2064 (1971).
[25] H.J.F. Jansen and A.J. Freeman, Phys. Rev. B **30**, 561 (1984); M. Weinert, H. Krakauer, E. Wimmer, and A.J. Freeman, *ibid.* **24**, 864 (1981).
[26] H.J. Monkhorst and J.D. Pack, Phys. Rev. B **13**, 5188 (1976).
[27] C.G. Broyden, Math. Comput. **19**, 577 (1965).
[28] *The Mathematical Theory of Symmetry in Solids*, edited by C.J. Bradley and A.P. Cracknell (Clarendon, Oxford, 1972); *International Tables for Crystallography*, edited by J. Hahn (Reidel, Dordrecht, 1983), Vol. A.
[29] R. Magri and C. Calandra, Phys. Rev. B **40**, 3896 (1989).
[30] *Electronic Structure and the Properties of Solids*, edited by W.A. Harrison (Freeman, San Francisco, 1980).
[31] *Numerical Data and Functional Relationships in Science and Technology—Crystal and Solid State Physics*, Vol. 77a of *Landolt-Börnstein*, edited by O. Madelung (Springer, Berlin, 1984).
[32] J.J. Hopfield, J. Phys. Chem. Solids **15**, 97 (1960).
[33] S. Massidda *et al.*, Phys. Rev. B **41**, 12 079 (1990).
[34] L. Hedin, Phys. Rev. **139**, A796 (1965).
[35] M.S. Hybertsen and S.G. Louie, Phys. Rev. Lett. **55**, 1418
[36] A. Svane and O. Gunnarsson, Phys. Rev. Lett. **65**, 1148 (1990).
[37] S.H. Wei and A. Zunger, Appl. Phys. Lett. **58**, 2685 (1991).